ORIGINAL ARTICLE

# Patient-specific simulations of transcatheter aortic valve stent implantation

C. Capelli · G. M. Bosi · E. Cerri · J. Nordmeyer ·
T. Odenwald · P. Bonhoeffer · F. Migliavacca ·
A. M. Taylor · S. Schievano

**Abstract** Transcatheter aortic valve implantation (TAVI) enables treatment of aortic stenosis with no need for open heart surgery. According to current guidelines, only patients considered at high surgical risk can be treated with TAVI. In this study, patient-specific analyses were performed to explore the feasibility of TAVI in morphologies, which are currently borderline cases for a percutaneous approach. Five patients were recruited: four patients with failed bioprosthetic aortic valves (stenosis) and one patient with an incompetent, native aortic valve. Three-dimensional models of the implantation sites were reconstructed from computed tomography images. Within these realistic geometries, TAVI with an Edwards Sapien stent was simulated using finite element (FE) modelling. Engineering and clinical outcomes were assessed. In all patients, FE analysis proved that TAVI was morphologically feasible. After the implantation, stress distribution showed no risks of immediate device failure and geometric orifice areas increased with low risk of obstruction of the coronary arteries. Maximum principal stresses in the arterial walls were higher in the model with native outflow tract. FE analyses can both refine patient selection and characterise device mechanical performance in TAVI, overall impacting on procedural safety in the early introduction of percutaneous heart valve devices in new patient populations.

**Keywords** Stent finite element analysis · Aortic valve stenosis · Transcatheter implantation · Patient-specific

C. Capelli (✉) · G. M. Bosi · E. Cerri · T. Odenwald ·
P. Bonhoeffer · A. M. Taylor · S. Schievano
Centre for Cardiovascular Imaging, UCL Institute of
Cardiovascular Science, Great Ormond Street Hospital for
Children, Great Ormond Street, London WC1N 3JH, UK
e-mail: c.capelli@ucl.ac.uk

G. M. Bosi · E. Cerri · F. Migliavacca
Laboratory of Biological Structure Mechanics, Structural
Engineering Department, Politecnico di Milano, Milan, Italy

J. Nordmeyer
Department of Congenital Heart Disease and Paediatric
Cardiology, Deutsches Herzzentrum Berlin, Berlin, Germany

## 1 Introduction

Aortic stenosis (AS) is currently the most common valve pathology in Europe and USA, where increased life expectancy is associated with degenerative diseases affecting cardiac structures [25]. Surgical valve replacement has been considered the gold standard for effectively treating AS [6]; however, the intrinsic invasive nature of open heart surgery exposes patients to high risks and slow recovery. Over the last decade, less invasive techniques have been introduced to insert cardiac valves using catheter-based interventions [5]. In 2002, the first intervention of transcatheter aortic valve implantation (TAVI) was successfully performed [9]. The possibility to replace cardiac valves using less invasive procedures has been a disruptive innovation and has revolutionised the treatment of patients with severe AS. Almost 10 years after the first case, two devices are commercially available for TAVI (Edwards Sapien, Edwards Lifesciences, Irvine, CA, USA; CoreValve®, Medtronic, Minneapolis, MN, USA) with over 40,000 cases reported and over 200 studies published, as recently presented at the 2011 Congress of European Society of Cardiology. Despite initial significant mortality and morbidity associated with TAVI, high rates of procedural success (94–97%) and acceptable procedure-related

complications (5–18%) are now being reported with favourable outcomes if compared with surgery [11, 30, 36, 43].

Nevertheless, the current guidelines still limit this relatively new technique to those patients who are considered at high or prohibitive risk for surgery. In contrast to most other medical procedures, which slowly progress from lower to higher risk patient populations, the course of TAVI has taken the opposite path [7, 44, 45].

In light of this, two conditions are considered in this study in order to potentially enlarge the population which could benefit from TAVI and, therefore, a less invasive approach to treatment of aortic valve dysfunction. First, degenerated surgical bioprostheses; repeated cardiac surgery to replace these valves has been shown to be technically challenging and associated with significant morbidity and operative mortality [16]. In this context, TAVI might be used as a second valve seated within the failed bioprosthetic valve [3, 27, 40, 41, 46]. To date, only a limited number of such valve-in-valve procedures have been reported in the literature. These procedures, for both stenosis and regurgitation, have mainly been performed with Edwards Sapien device [4]. However, despite proven feasibility, data are still preliminary and no precise guidelines have been recommended [44]. Second, patients with congenital heart disease and low surgical risk, who are excluded under the current TAVI guidelines [36]; in this group of patients, TAVI might be introduced [13] to reduce the number of open heart surgeries that they have to undergo over their life.

In order to explore the feasibility of this intervention in the above-mentioned patient populations, preclinical testing and accurate pre-procedural evaluation are crucial. Engineering approaches may be used to improve procedural safety [1, 26, 29]. By combining high-resolution imaging techniques [42] and finite element (FE) analyses [35], virtual implantation of such devices is possible in order to understand the interaction of the device with the complex anatomical environment for individual patients. So-called patient-specific models of medical devices can play an important role in improving cardiovascular interventions. Simulations which consider the morphological human variability between subjects can provide invaluable projections on the in vivo performance and overcome the limitations of idealised experimental settings [38].

Patient-specific simulations have already been used to predict the outcome of percutaneous valve implantations and effectively help develop a new pulmonary procedure [33, 34]; however, to the best of our knowledge, these methodologies have not been applied to the aortic valve.

In this study, FE analyses were performed to explore the feasibility of TAVI in specific patient morphologies which are currently borderline cases for a percutaneous approach.

This method can help in both refining patient selection and characterising device mechanical performance, overall impacting on procedural safety and success in the early introduction of TAVI devices in new patient populations [21].

## 2 Methods

Finite element analyses were implemented by modelling the following components: implantation site of five specific patients, four different bioprosthetic aortic valves, a balloon-expandable TAVI stent, and an angioplasty balloon.

### 2.1 Patient-specific implantation sites

Five patients, who were referred for surgical replacement of the aortic valve, were recruited for this study: four patients with four different, stenotic bioprosthetic valves (patients A, B, C, D) and one patient with incompetent, native aortic valve (patient E).

The study was approved by the local ethics committee, and all patients gave informed consent to be included in the study and for use of their anonymised data.

Patient A was previously diagnosed with severe AS and underwent surgical aortic valve replacement with a 23 mm Carpentier-Edwards Perimount Magna valve (Edwards Lifesciences). Two years later, the bioprosthetic aortic valve had undergone calcific restenosis.

Patient B was diagnosed with moderate to severe AS. The patient underwent surgical aortic valve replacement with a 23 mm Soprano$^{TM}$ valve (Sorin Biomedica Cardio, Saluggia, Italy). During the third year of follow-up, evidence of restenosis was diagnosed.

Patient C had critical AS. Surgery was performed to replace his aortic valve with a 25 mm Carpentier-Edwards Perimount valve (Edwards Lifesciences). At the 5-year follow-up, AS had recurred.

Patient D was diagnosed with moderate to severe AS. During the surgical intervention, a bicuspid calcified aortic valve was replaced with a 25 mm Epic$^{TM}$ valve (St Jude Medical, St Paul, MN, USA). At 1-year follow-up, AS was noticed.

Patient E was diagnosed with congenital tricuspid aortic valve stenosis with mild–moderate obstruction at birth, which was treated with aortic balloon valvuloplasty. At 21 years of age, the patient was referred to surgery because of severe aortic regurgitation.

Image data of left ventricular outflow tract (LVOT), aortic root, coronary arteries, aortic valve leaflets and bioprostheses (patients A–D) were acquired for each patient using Dual-source, 64-slice computed tomography (CT-SOMATOM Definition, Siemens Medical Solutions,

Forchheim, Germany). Retrospective CT scanning with dose modulation was performed to acquire ten three-dimensional (3D) images throughout the cardiac cycle [31]. Images corresponding to mid-systole (i.e. open aortic valve leaflets) were identified in each patient and were imported into the image post-processing software Mimics (Materialise, Materialise Inc., Leuven, Belgium). 3D models of each implantation site (Fig. 1) were obtained according to previously described methodologies [32].

Aortic wall and native valve leaflets were assumed to be, respectively, 2 and 0.5 mm thick [8, 28] with a density equal to 1,120 kg/m$^3$ for all models. To describe the mechanical behaviour of the aortic root in the FE model, a Mooney–Rivlin hyperelastic constitutive law was adopted incorporating experimental stress–strain data from the ascending aorta [24]. Residual stresses (400 kPa) were included in the model to take into account the pre-stretching of the aortic root [18]. The aortic roots were meshed with 3D triangular shell general-purpose elements. Table 1 summarises the number of elements used for each model.

### 2.2 Bioprosthetic aortic valves

The metal frames of the four bioprosthetic valves were reconstructed from the CT images to identify their position inside the patients' outflow tracts. Bioprosthetic valve geometries were then re-drawn with CAD software (Rhinoceros 4.0, Robert McNeel, Seattle, WA, USA) to recreate a complete model of the corresponding commercial device used in the patients, and placed in the same position as that identified from CT images. Each design included different sewing rings and valve leaflets:

- The Carpentier-Edwards Perimount Magna valve had a lower ring of 2 mm in height with a rectangular, 0.5 mm thick section. The upper support had a circular section with a diameter of 0.5 mm. The total height of the valve was 14.5 mm and the diameter 23 mm (Fig. 2).

- The Soprano$^{TM}$ valve had a lower ring of 2.5 mm in height, a rectangular, 0.5 mm thick section. The support was totally filled, and the upper section was semi-circular with a radius of 0.25 mm. The total height of the valve was 14.5 mm and the diameter 23 mm.
- The Carpentier-Edwards Perimount valve had a lower ring of 2.15 mm in height with a rectangular, 0.54 mm thick section. The upper support had a circular section with a diameter of 0.54 mm. The total height of the valve was 15.7 mm and the diameter 25 mm.
- The Epic$^{TM}$ valve had a lower ring of 2.72 mm in height with a rectangular, 0.54 mm thick section. The upper support had a circular section with a diameter of 0.54 mm. The total height of the valve was 15.7 mm and the diameter 25 mm.

Material properties were determined from available manufacturers' data. The metallic frames of both Perimount devices were modelled using an elasto-plastic constitutive law (density 8,300 kg/m$^3$, Young's modulus 189,600 MPa, yield stress 760 MPa, ultimate stress 1,160 MPa). The polymeric frames of Soprano$^{TM}$ and Epic$^{TM}$ valves were described by elasto-plastic parameters (density 9,120 kg/m$^3$, Young's modulus 2,840 MPa, yield stress 65.4 MPa, ultimate stress 358 MPa).

The three aortic valve leaflets were included in each FE model of the prosthetic valve. Leaflets of bovine pericardium origin are mounted on the Soprano$^{TM}$ and Perimount valves, while porcine leaflets are used in the Epic$^{TM}$ valve. Both bovine and porcine leaflets were simplified with a linear, elastic model (bovine: density 1,120 kg/m$^3$, Young's modulus 6 MPa; porcine: density 1,120 kg/m$^3$, Young's modulus 7.5 MPa) by elaborating the results of experimental studies [19, 47]. Calcification of the leaflets was created by increasing Young's modulus and thickness, respectively, to 10 MPa and 1.4 mm in the region of the commissures [22], where a weld constraint was also applied; 16 connector elements per commissure were added. An axial, rigid behaviour was assigned to the connectors, allowing them to maintain a fixed distance between
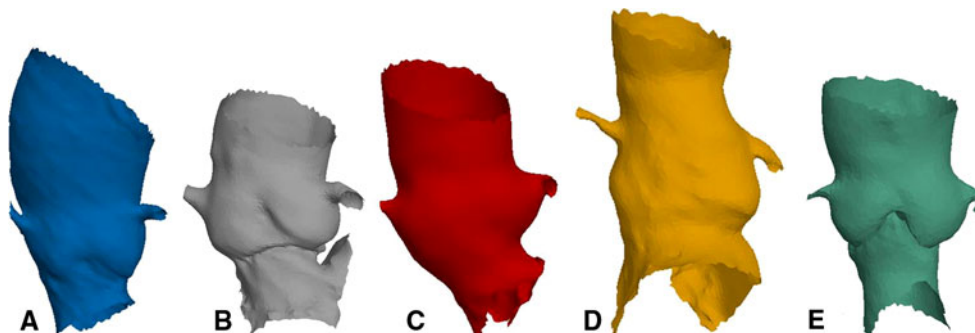


**Fig. 1** From *left* to *right*, 3D volumetric reconstructions of the five selected patients' aortic roots

**Table 1** Mesh number of elements of the parts involved in the FE simulations

| Part | Elements |
|---|---|
| Patient-specific model | |
| A | 6,875 |
| B | 8,675 |
| C | 11,325 |
| D | 8,347 |
| E | 18,890 |
| Bioprostheses (stent + leaflet) | |
| Perimount Magna | 44,048 + 29,021 |
| Soprano™ | 51,372 + 28,667 |
| Perimount | 44,048 + 29,021 |
| Epic™ | 51,372 + 28,667 |
| TAVI device | |
| Sapien stent | 192,920 |
| Balloon | 8,160 |
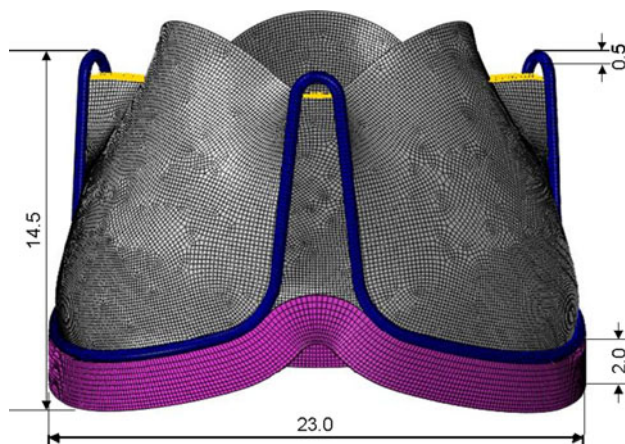


**Fig. 2** Carpentier-Edwards Perimount Magna bioprosthetic valve FE model and dimensions (mm): *lower* (*purple*) and *upper* (*blue*) support rings; valve leaflets (*grey*) and connector elements (*yellow*) to simulate the calcification (colour figure online)

the two nodes until a threshold force was reached—equal to 0.92 N [22] along the direction joining the 2 nodes—and then fail after this threshold value was reached mimicking calcification failure. The thickening and welding of the failing valve leaflets produced aortic valve geometric orifice areas equal to those measured in the selected patients (1.2 cm$^2$ for A and B, and 1.4 cm$^2$ for C and D). The rigid supports of the valves were meshed using 8-node linear hexahedral elements with reduced integration with a number of elements varying from 28,667 to 29,021 according to the model (Table 1). The valve leaflets were meshed with 4-node, quadrilateral, shell elements with reduced integration and large-strain formulation (Fig. 2).

### 2.3 TAVI device

Model of TAVI stent was drawn resembling the Edwards Sapien device; the presence of the valve was excluded from this study. This stent is characterised by 12 units, each formed by 4 zigzag elements (Fig. 3). A vertical bar divides each unit and a perforated bar is positioned every 4 units. The TAVI device was chosen to have a nominal external diameter (=26 mm) > the internal diameter of the failing bioprosthetic valves; the height and thickness of the expanded stent were 16 and 0.3 mm, respectively.

Mechanical behaviour of the stent material was based on a homogeneous, isotropic, elasto-plastic austenitic stainless steel. The adopted constitutive law was a Von Mises plasticity model (density 8,000 kg/m$^3$, Young's modulus 193,000 MPa, yield stress 205 MPa, ultimate stress 515 MPa) with an initial linear elastic response followed by a plastic isotropic hardening behaviour obtained from experimental data [2]. The stent was meshed with 192,920 hexahedral elements, following mesh sensitivity analysis.

### 2.4 Balloon

The geometry of the balloon was drawn in the expanded configuration to resemble the geometry of the commercial balloon (Z MED II™, NuMed Inc., Hopkinton, NY, USA) used in clinical practice [17]. The nominal length of the expanded balloon was 50 mm; the cylindrical body that is in contact with the stent had a nominal diameter of 21.85 mm and length of 30 mm. The geometry of the deflated balloon was obtained according to previously published work [13].

A homogeneous, isotropic, linear elastic Nylon11 was adopted as per manufacturer's data (density 1,256 kg/m$^3$, Young's modulus 450 MPa). The balloon was meshed with 0.03 mm thick membrane elements with an average size of
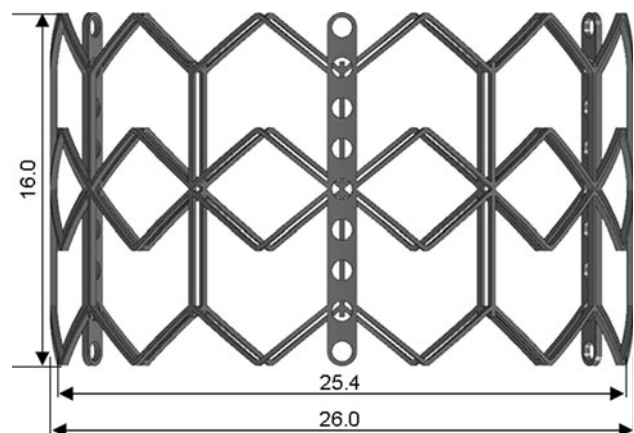


**Fig. 3** CAD model and dimensions of the recreated Edwards Sapien stent (mm)

1 mm in the longitudinal direction and 0.5 mm in the circumferential direction.

## 2.5 Analyses

Large deformation analyses of TAVI were performed using Abaqus/Explicit 6.9 (Simulia, Providence, RI, USA).

In models $A$–$D$, the device was positioned coaxially within the outflow portion, overlapping the sewing ring of the surgically implanted prosthesis according to clinical indications [46]. In these patients, connector elements were used to link the re-drawn bioprosthetic valves with the aortic vessels to mimic the suture between the ring and the aortic root.

In model $E$, the stent was placed in three different positions within the LVOT/aortic root to test the influence of the landing zone into safe anchoring, the interaction with other cardiac structures and potential occlusion of the coronary arteries. First, the central section of the stent was placed aligned to the leaflet commissures ($E_M$; Fig. 4), then it was moved 4.2 mm proximally towards the left ventricle ($E_P$; Fig. 4), and 4.2 mm distally towards the aortic arch ($E_D$; Fig. 4).

The Sapien stent was designed in its expanded configuration and crimped onto the balloon to the size of the catheter (8 mm diameter) using a coaxial cylindrical surface. The stent deployment was divided into two different steps: balloon pressurisation (0.342 MPa) with resulting stent expansion in the LVOT, and balloon deflation with subsequent stent recoil. In all patients, the LVOT/aortic root extremities (upper and lower aortic sections and coronary terminal sections) were constrained in all directions (circumferential, radial and longitudinal) in order to mimic the connection with biological structures. Boundary conditions on the balloon were placed to mimic the bond with the catheter.

Contact properties were defined to describe the interactions encountered in these multi-part analyses. Friction between Nylon and stainless steel was included in the model with coefficient equal to 0.25 [10]. Interactions included contact between surfaces belonging to balloon and stent, balloon and bioprosthetic aortic valve leaflets, stent and bioprosthetic aortic valve, bioprosthetic aortic valve and aortic wall.

The following quantities of interests were measured in order to evaluate the mechanical performance of the stent and the overall impact of the TAVI device into the selected patient-specific models:

- stent configuration at the end of balloon inflation and deflation, and interaction with other cardiac structures,
- stent recoil, measured as a percentage of diameter change before and after balloon deflation,
- stent Von Mises stress distribution at the end of the simulated implant,
- post-TAVI geometric orifice area, measured as the cross-sectional area of the stent at the smaller section,
- obstruction of the coronary arteries, evaluated according to the minimum distance of the Sapien device/aortic valve leaflets from the coronary ostia,
- comparison of maximum principal stress distribution in the arterial walls.

## 3 Results

At the end of all simulations, the TAVI stent was virtually implanted in the five patient-specific aortic root models. Inside the four models with bioprosthetic valves ($A$–$D$), the stent deployed symmetrically against the sewing rings and valve leaflets, with no contact with the native aortic wall and/or other cardiac structure (Fig. 5). In model $E$, the



**Fig. 4** Balloon and TAVI stent in the three analysed positions inside the native aortic valve: the central section of the stent placed in correspondence of the leaflet commissures ($E_M$); moved 4.2 mm proximally towards the left ventricle ($E_P$); and, 4.2 mm distally towards the aortic arch ($E_D$)
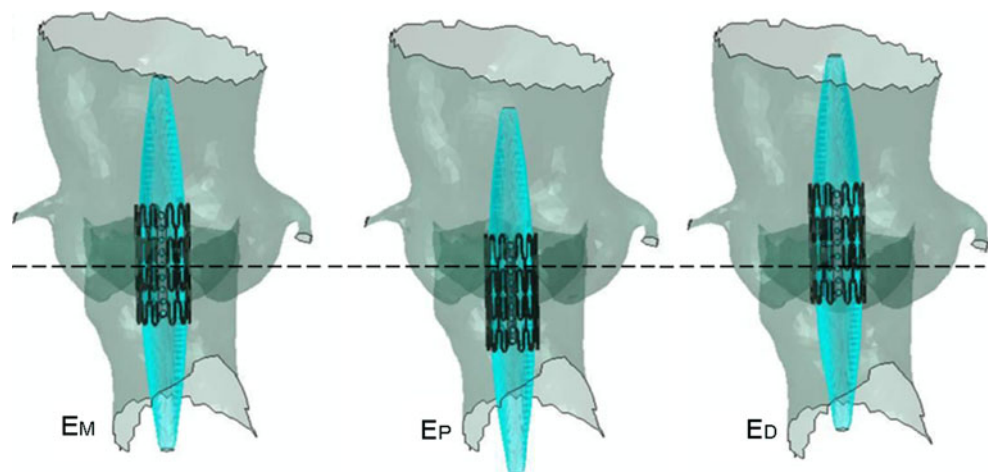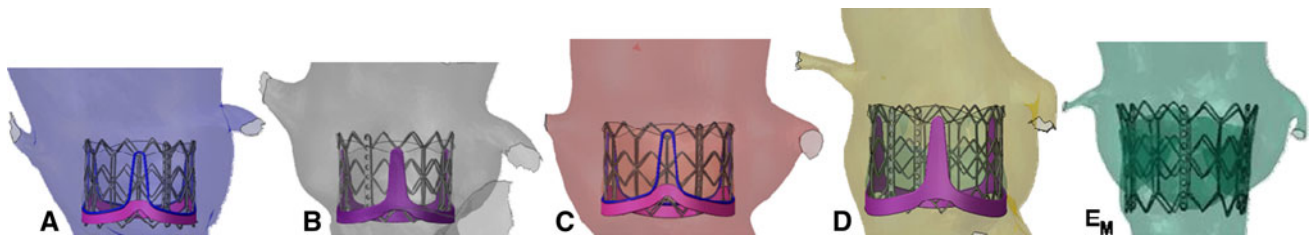
**Fig. 5** TAVI stent final configuration (end of balloon deflation) for models $A$–$D$ and $E_M$

device assumed an asymmetrical configuration for the three tested positions, more open distally than proximally ($E_M$ in Fig. 5). In all three cases, the interaction between the TAVI device and the native implantation site was well confined within the LVOT and aortic root portion of the patient's morphology, thus reducing the potential risk of heart block and mitral valve leaflet entrapment.

Stent radial recoil was recorded after balloon deflation. In all the models including bioprosthetic valves the maximum recoil was measured in the distal sections towards the aortic arch (model $A = 17.0\%$, model $B = 13.2\%$, model $C = 11.7\%$, model $D = 10.8\%$). Recoil was absent or low proximally, at the level of the bioprosthetic valves' annulus (model $A = 0.0\%$, model $B = 1.7\%$, model $C = 1.7\%$, model $D = 0.0\%$). In the model with the native valve, the maximum recoil was measured proximally, in the portions of stent mostly interacting with the LVOTs (model $E_M = 14.9\%$; model $E_P = 20.2\%$; model $E_D = 11.4\%$).

The highest Von Mises stresses occurred at the strut junctions for all the models. The maximum reached values were included between 414 MPa (model $E_D$) and 477 MPa (model $E_P$, in Fig. 6). Stress values throughout the length of the stent zigzags and vertical bars were lower than 250 MPa. Material plasticisation occurred at the points of maximum stresses, i.e. at the junctions between zigzag and vertical bars, thus guaranteeing a final open configuration of the stent.

In models $A$–$D$, the axial connector elements representing the welding constraint caused by the calcification at the leaflet commissure levels were broken during the inflation of the stent–balloon system. Geometric orifice area increased from 1.2 cm$^2$ to 3.4 and 3.6 cm$^2$ in models $A$ and $B$, respectively, and from 1.4 to 3.7 cm$^2$ in models $C$ and $D$. The final geometric orifice areas in the three positions $E_M$, $E_P$ and $E_D$ were, respectively, 4.7, 3.7 and 5.3 cm$^2$ compared to an initial orifice of 3.7 cm$^2$.

The minimum distances between the closest stent strut/bioprosthetic valve leaflet and coronary ostia are reported in Table 2. In none of the models, direct obstruction of the coronaries occurred; neither the TAVI stent nor the bioprosthetic valve leaflets occluded the ostia. The stent positioned in model $D$ was the closest (5.5 mm) to the coronaries amongst those with bioprosthetic valves. The distal position of the stent implanted in model $E_D$ was the closest to the right coronary artery (3.1 mm) amongst the three positions tested.

In all models with bioprosthetic valves, the principal stress state in the aortic root reached the maximum value of 0.1 MPa, while in model $E$ the maximum principal stress in the LVOT was higher, showing how the implanted bioprostheses act as a scaffold for the TAVI stent. By comparing the stress distribution induced by the three stent positions in patient E, higher stresses were found in the

**Fig. 6** Von Mises stress distribution in the TAVI stent after balloon deflation in model $E_P$
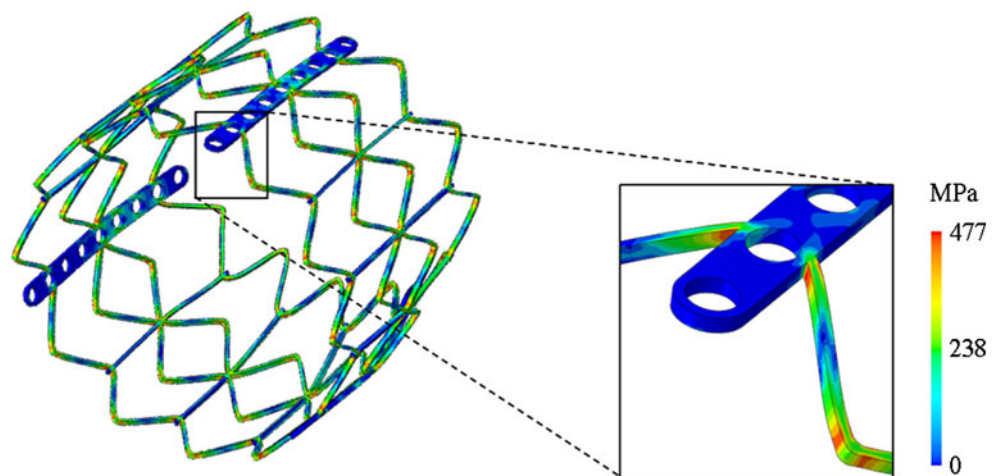
**Table 2** Distance between the implanted TAVI device and the coronary arteries (right and left) after balloon deflation in the selected patient's models

| Model | Distance Sapien-right coronary artery (mm) | Distance Sapien-left coronary artery (mm) |
|---|---|---|
| A | 13.6 | 10.9 |
| B | 14.1 | 11.4 |
| C | 14.3 | 10.5 |
| D | 6.2 | 5.5 |
| $E_M$ | 4.3 | 5.6 |
| $E_P$ | 6.2 | 7.9 |
| $E_D$ | 3.1 | 6.1 |

Models A–D refer to patients with stenotic bioprosthetic valves. Models $E_M$, $E_P$ and $E_D$ refer to the patient with the native valve where the stent was implanted, respectively, in correspondence of the leaflet commissures, proximally towards the left ventricle and distally towards the aortic arch

leaflet regions of model $E_D$, especially at the commissure level (Fig. 7).

## 4 Discussion

In this study, a detailed FE model of TAVI has been developed; a balloon-expandable device (Sapien) was successfully deployed in five patient-specific morphologies of LVOT/aortic root—four of them included a biprosthetic valve previously implanted via conventional surgery and one had a regurgitant native aortic valve. Using FE analysis, the effects of the implantation phases on mechanical performance of the device were investigated and potential clinical outcomes were derived. To the best of our knowledge, there are no studies to date that combined FE methods with clinical data to simulate TAVI.

Patient-specific FE analyses might help engineers to better understand the stresses on the stent when interacting with a wide variety of potential anatomies and, therefore, to optimise the device design for a range of potential clinical applications.

By analysing the stent configuration after the simulated procedure, stress differences were quantified under different conditions (i.e. different patient, different bioprostheses).

In all cases, geometrical asymmetries led to a non-uniform stress distribution on the stent struts. By taking into account the interaction with artificial and biological structures, elastic recoil up to 20% was measured after balloon deflation. Distal and proximal recoils were associated with bioprosthetic and native valves, respectively. This difference can be explained with the influence of the interacting structures in the two analysed situations: metallic or polymeric frames which stiffen the proximal portion of the implantation sites in the first case, and elastic LVOT in the native implantation site. These results were found to be in good agreement with available clinical data of TAVI follow-up [20]. In clinical practice, these results should be taken into account to prevent obstruction of the LVOT and dislodgement of TAVI device. By examining Von Mises stress distribution, a final open configuration of the stent was guaranteed by material plasticisation which occurred in correspondence to strut junctions. The ultimate stress value for stainless steel AISI 316L (i.e. 515 MPa) was not reached; this means that no stent fractures were seen immediately after deployment. The non-uniform shape of the deployed configuration and, therefore, the asymmetric stress distribution might still cause long-term stent failure due to the pulsatile loading conditions during the cardiac cycle [34].

It has been reported that coronary obstruction may occur as a consequence of transcatheter valve-in-valve implantation [15]. With the presented computational approach, an assessment of this risk could be quantified. By measuring the distance between device and coronary ostia, in three models (i.e. A, B and C) comparable values with physiological distances from native aortic valve leaflets (i.e. 12 mm [39]) have been found. In model D, the device is closer to the coronaries. The stent implanted in the most distal position in model $E_D$ is the closest (3.1 mm) to the coronaries. Further fluid dynamic analyses could study in depth the potential interference of the TAVI device to the coronary flow [23].

Finally, by analysing stress state on the aortic wall, the stress peak was found up to ten times higher in patient E than in patients with bioprosthetic valves. The implanted prosthesis probably protects the artery from the load imposed by the TAVI stent expansion, avoiding direct contact with it. Conversely, in patient E, the stent interacted



**Fig. 7** Maximum principal stress distribution in the native aortic valve leaflets and aortic root after balloon deflation in models $E_M$, $E_P$ and $E_D$
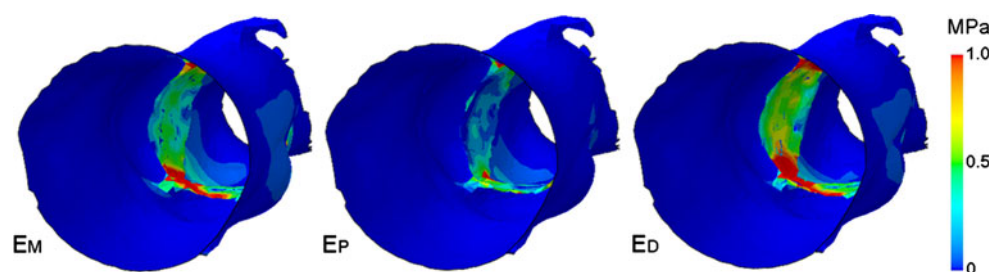
directly with the vascular wall. The stent placed in the most distal position (model $E_D$) caused the highest stresses in the leaflet regions where it might induce damage or stimulate remodelling.

This study has some clinical implications. The analyses performed in this work confirmed that TAVI can theoretically be performed safely in patients with failed bioprostheses. The feasibility of this procedure has already been demonstrated. However, clinical data about potential combinations of available surgical and transcatheter valve types and sizes are still not available. Hence, patient-specific computational analyses have been used to explore some of the multiple possibilities of TAVI devices in bioprosthetic heart valves and concurrently address clinically relevant questions. For example, little is known about the risk of coronary obstruction with valve-in-valve implantation and predicting the correct device size to avoid this adverse event can be extremely challenging [46].

In addition, TAVI feasibility was verified inside the aortic morphology of a young patient with an incompetent native aortic valve. The clinical assessment of TAVI in this particular population is in its infancy [14] and numerical simulations might support procedural planning, by helping choose the optimal position for each individual patient, as shown by our study. Indeed, the results of the presented simulations proved that the subject might be suitable for this treatment, but, while the landing zone for patients with bioprosthetic valve is clearly outlined, the effects of the positioning in the case of native implantation sites need to be taken into account to avoid interference with other cardiac structures and high stress distributions in the device.

Despite the attempt of realistically replicate the complex environment of a percutaneous procedure, these FE models still present limitations.

Though our data for the use of computational modelling in TAVI are encouraging, the limited number of patients analysed in this study still means that computational simulations will not be used routinely in clinical practice. Additional integrated clinical studies have to be planned to validate the robustness of this methodology and the computational results against the outcomes from treated patient populations. However, proof of concept has been demonstrated in this study on cases which differ in morphologies, type of failed bioprostheses and material properties.

The aortic root reconstructed for this study was patient-specific in terms of geometry, but not in terms of material constitutive behaviour. A better characterisation of each patient implantation site physical properties would allow us to replicate the individual response of the arterial wall to TAVI. Analogous considerations can be drawn on the calcification model; in this study, the presence of stenotic valve leaflets was simulated by thickening of the leaflets and by a welding constraint placed symmetrically at the commissures. To date, there are few specific data in literature for aortic valve calcification material, mainly because of its great variability in composition (degree of calcification and presence of lipids) and the difficulty to mechanically characterise this type of tissue. In light of this, only comparative conclusions could be drawn in terms of stress distribution in the arterial wall model.

TAVI valve leaflets were excluded from the model of the device as only the implantation procedure was simulated. Therefore, hemodynamics of the TAVI valve and consequences of migration forces on the stent [12] could not be assessed. In addition, effective orifice area, as based on calculation from flow-jet downstream of the aortic valve, could not be evaluated. Alternatively, in this study, the measure of geometric orifice area provided an indication of the potential clinical success of the procedure. Bearing this in mind, the next aim will be taking into account the interaction of fluid and structure in order to consider the presence of the blood, to integrate the effects of further recoil force due to the pressure load on the leaflets, assess potential valvular and para-valvular leakage [37], and predict the risk of embolisation and long-term performance.

In conclusion, a further integrated clinical study needs to be planned to verify the findings of this methodology against the outcome of treated patient populations and to support a safer development of TAVI using realistic numerical simulations.

## References

1. Antiga L, Piccinelli M, Botti L, Ene-Iordache B, Remuzzi A, Steinman DA (2008) An image-based modeling framework for patient-specific computational hemodynamics. Med Biol Eng Comput 46:1097–1112
2. Auricchio F, Di Loreto M, Sacco E (2001) Finite-element analysis of a stenotic artery revascularization through a stent insertion. Comput Methods Biomech Biomed Eng 4:249–263
3. Azadani AN, Jaussaud N, Matthews PB, Ge L, Chuter TAM, Tseng EE (2010) Transcatheter aortic valves inadequately relieve stenosis in small degenerated bioprostheses. Interact Cardiovasc Thorac Surg 11:70–77
4. Azadani AN, Tseng EE (2010) Transcatheter valve-in-valve implantation for failing bioprosthetic valves. Future Cardiol 6:811–831
5. Bonhoeffer P, Boudjemline Y, Saliba Z, Merckx J, Aggoun Y, Bonnet D, Acar P, Le Bidois J, Sidi D, Kachaner J (2000) Percutaneous replacement of pulmonary valve in a right-ventricle to pulmonary-artery prosthetic conduit with valve dysfunction. Lancet 356:1403–1405

6. Buellesfeld L, Windecker S (2011) Transcatheter aortic valve implantation: the evidence is catching up with reality. Eur Heart J 32:133–137

7. Carabello BA (2010) Percutaneous therapy for valvular heart disease a huge advance and a huge challenge to do it right. Circulation 121:1798–1799

8. Conti CA, Votta E, Della Corte A, Del Viscovo L, Bancone C, Cotrufo M, Redaelli A (2010) Dynamic finite element analysis of the aortic root from MRI-derived parameters. Med Eng Phys 32:212–221

9. Cribier A, Eltchaninoff H, Bash A, Borenstein N, Tron C, Bauer F, Derumeaux G, Anselme F, Laborde F, Leon MB (2002) Percutaneous transcatheter implantation of an aortic valve prosthesis for calcific aortic stenosis—first human case description. Circulation 106:3006–3008

10. De Beule M, Mortier P, Carlier SG, Verhegghe B, Van Impe R, Verdonck P (2008) Realistic finite element-based stent design: the impact of balloon folding. J Biomech 41:383–389

11. Delgado V, Ewe SH, Ng ACT, van der Kley F, Marsan NA, Schuijf JD, Schalij MJ, Bax JJ (2010) Multimodality imaging in transcatheter aortic valve implantation: key steps to assess procedural feasibility. Eurointervention 6:643–652

12. Dwyer HA, Matthews PB, Azadani A, Ge L, Guy TS, Tseng EE (2009) Migration forces of transcatheter aortic valves in patients with noncalcific aortic insufficiency. J Thorac Cardiovasc Surg 138:1227–1233

13. Gervaso F, Capelli C, Petrini L, Lattanzio S, Di Virgilio L, Migliavacca F (2008) On the effects of different strategies in modelling balloon-expandable stenting by means of finite element method. J Biomech 41:1206–1212

14. Godin M, Borz B, Tron C, Durand E, Doguet F, Litzler P-Y, Bessou J-P, Cribier A, Eltchaninoff H (2011) Transcatheter aortic valve implantation with the Edwards valve prosthesis in patients with low (<20%) logistic Euroscore: results of a prospective Single Center Registry. Eur Heart J 32:903

15. Gurvitch R, Cheung A, Bedogni F, Webb JG (2011) Coronary obstruction following transcatheter aortic valve-in-valve implantation for failed surgical bioprostheses. Catheter Cardiovasc Interv 77:439–444

16. Jones JM, O'Kane H, Gladstone DJ, Sarsam MAI, Campalani G, MacGowan SW, Cleland J, Cran GW (2001) Repeat heart valve surgery: risk factors for operative mortality. J Thorac Cardiovasc Surg 122:913–918

17. Kahlert P, Eggebrecht H, Plicht B, Kraff O, McDougall I, Decker B, Erbel R, Ladd ME, Quick HH (2010) Towards real-time cardiovascular magnetic resonance-guided transarterial aortic valve implantation: in vitro evaluation and modification of existing devices. J Cardiovasc Magn Reson 12

18. Labrosse MR, Beller CJ, Mesana T, Veinot JP (2009) Mechanical behavior of human aortas: experiments, material constants and 3-d finite element modeling including residual stress. J Biomech 42:996–1004

19. Lee JM, Boughner DR, Courtman DW (1984) The glutaraldehyde-stabilized porcine aortic-valve xenograft. II. Effect of fixation with or without pressure on the tensile viscoelastic properties of the leaflet material. J Biomed Mater Res 18:79–98

20. Leipsic J, Gurvitch R, LaBounty TM, Min JK, Wood D, Johnson M, Ajlan AM, Wijesinghe N, Webb JG (2011) Multidetector computed tomography in transcatheter aortic valve implantation. J Am Coll Cardiol Imaging 4:416–429

21. Leon MB, Piazza N, Nikolsky E, Blackstone EH, Cutlip DE, Kappetein AP, Krucoff MW, Mack M, Mehran R, Miller C, Morel M-a, Petersen J, Popma JJ, Takkenberg JJM, Vahanian A, van Es G-A, Vranckx P, Webb JG, Windecker S, Serruys PW (2011) Standardized endpoint definitions for transcatheter aortic valve implantation clinical trials a consensus report from the valve academic research consortium. J Am Coll Cardiol 57:253–269

22. Loree HM, Grodzinsky AJ, Park SY, Gibson LJ, Lee RT (1994) Static circumferential tangential modulus of human atherosclerotic tissue. J Biomech 27:195–204

23. Nicosia MA, Cochran RP, Einstein DR, Rutland CJ, Kunzelman KS (2003) A coupled fluid-structure finite element model of the aortic valve and root. J Heart Valve Dis 12:781–789

24. Okamoto RJ, Wagenseil JE, DeLong WR, Peterson SJ, Kouchoukos NT, Sundt TM (2002) Mechanical properties of dilated human ascending aorta. Ann Biomed Eng 30:624–635

25. Otto CM (2008) Calcific aortic stenosis—time to look more closely at the valve. N Engl J Med 359:1395–1398

26. Padala M, Sarin E, Willis P, Babaliaros V, Block P, Guyton R, Thourani V (2010) An engineering review of transcatheter aortic valve technologies. Cardiovasc Eng Technol 1:77–87

27. Piazza N, Bleiziffer S, Brockmann G, Hendrick R, Deutsch M-A, Opitz A, Mazzitelli D, Tassani-Prell P, Schreiber C, Lange R (2011) Transcatheter aortic valve implantation for failing surgical aortic bioprosthetic valve from concept to clinical application and evaluation (part 2). JACC Cardiovasc Interv 4:733–742

28. Ranga A, Mongrain R, Galaz RM, Biadillah Y, Cartier R (2004) Large-displacement 3d structural analysis of an aortic valve model with nonlinear material properties. J Med Eng Technol 28:95–103

29. Ricotta JJ, Pagan J, Xenos M, Alemu Y, Einav S, Bluestein D (2008) Cardiovascular disease management: the need for better diagnostics. Med Biol Eng Comput 46:1059–1068

30. Rodes-Cabau J, Webb JG, Cheung A, Ye J, Dumont E, Feindel CM, Osten M, Natarajan MK, Velianou JL, Martucci G, DeVarennes B, Chisholm R, Peterson MD, Lichtenstein SV, Nietlispach F, Doyle D, DeLarochelliere R, Teoh K, Chu V, Dancea A, Lachapelle K, Cheema A, Latter D, Horlick E (2010) Transcatheter aortic valve implantation for the treatment of severe symptomatic aortic stenosis in patients at very high or prohibitive surgical risk acute and late outcomes of the multicenter canadian experience. J Am Coll Cardiol 55:1080–1090

31. Schievano S, Capelli C, Young C, Lurz P, Nordmeyer J, Owens C, Bonhoeffer P, Taylor AM (2011) Four-dimensional computed tomography: a method of assessing right ventricular outflow tract and pulmonary artery deformations throughout the cardiac cycle. Eur Radiol 21:36–45

32. Schievano S, Migliavacca F, Coats L, Khambadkone S, Carminati M, Wilson N, Deanfield JE, Bonhoeffer P, Taylor AM (2007) Percutaneous pulmonary valve implantation based on rapid prototyping of right ventricular outflow tract and pulmonary trunk from mr data. Radiology 242:490–497

33. Schievano S, Taylor AM, Capelli C, Coats L, Walker F, Lurz P, Nordmeyer J, Wright S, Khambadkone S, Tsang V, Carminati M, Bonhoeffer P (2010) First-in-man implantation of a novel percutaneous valve: a new approach to medical device development. Eurointervention 5:745–750

34. Schievano S, Taylor AM, Capelli C, Lurz P, Nordmeyer J, Migliavacca F, Bonhoeffer P (2010) Patient specific finite element analysis results in more accurate prediction of stent fractures: application to percutaneous pulmonary valve implantation. J Biomech 43:687–693

35. Schoenhagen P, Hill A, Kelley T, Popovic Z, Halliburton SS (2011) In vivo imaging and computational analysis of the aortic root. Application in clinical research and design of transcatheter aortic valve systems. J Cardiovasc Trans Res 4:459–469

36. Smith CR, Leon MB, Mack MJ, Miller C, Moses JW, Svensson LG, Tuzcu EM, Webb JG, Fontana GP, Makkar RR, Williams M, Dewey T, Kapadia S, Babaliaros V, Thourani VH, Corso P, Pichard AD, Bavaria JE, Herrmann HC, Akin JJ, Anderson WN, Wang D, Pocock SJ, Investigators PT (2011) Transcatheter

versus surgical aortic-valve replacement in high-risk patients. N Engl J Med 364:2187–2198

37. Sun W, Li K, Sirois E (2010) Simulated elliptical bioprosthetic valve deformation: implications for asymmetric transcatheter valve deployment. J Biomech 43:3085–3090

38. Taylor CA, Figueroa CA (2009) Patient-specific modeling of cardiovascular mechanics. Annu Rev Biomed Eng 11:109–134

39. Tops LF, Wood DA, Delgado V, Schuijf JD, Mayo JR, Pasupati S, Lamers FPL, van der Wall EE, Schalij MJ, Webb JG, Bax JJ (2008) Noninvasive evaluation of the aortic root with multislice computed tomography implications for transcatheter aortic valve replacement. J Am Coll Cardiol Img 1:321–330

40. Walther T, Dehdashtian MM, Khanna R, Young E, Goldbrunner PJ, Lee W (2011) Trans-catheter valve-in-valve implantation: in vitro hydrodynamic performance of the sapien + cloth trans-catheter heart valve in the carpentier-edwards perimount valves. Eur J Cardiothorac Surg 40:1120–1126

41. Walther T, Falk V, Dewey T, Kempfert J, Emrich F, Pfannmueller B, Broeske P, Borger MA, Schuler G, Mack M, Mohr FW (2007) Valve-in-a-valve concept for transcatheter minimally invasive repeat xenograft implantation. J Am Coll Cardiol 50:56–60

42. Wang Q, Book G, Contreras Ortiz S, Primiano C, McKay R, Kodali S, Sun W (2011) Dimensional analysis of aortic root geometry during diastole using 3d models reconstructed from clinical 64-slice computed tomography images. Cardiovasc Eng Technol 2:324–333

43. Webb J, Cribier A (2011) Percutaneous transarterial aortic valve implantation: what do we know? Eur Heart J 32:140–147

44. Webb JG, Altwegg L, Boone RH, Cheung A, Ye J, Lichtenstein S, Lee M, Masson JB, Thompson C, Moss R, Carere R, Munt B, Nietlispach F, Humphries K (2009) Transcatheter aortic valve implantation impact on clinical and valve-related outcomes. Circulation 119:3009–3016

45. Webb JG, Lichtenstein S (2007) Transcatheter percutaneous and transapical aortic valve replacement. Semin Thorac Cardiovasc Surg 19:304–310

46. Webb JG, Wood DA, Ye J, Gurvitch R, Masson J-B, Rodes-Cabau J, Osten M, Horlick E, Wendler O, Dumont E, Carere RG, Wijesinghe N, Nietlispach F, Johnson M, Thompson CR, Moss R, Leipsic J, Munt B, Lichtenstein SV, Cheung A (2010) Trans-catheter valve-in-valve implantation for failed bioprosthetic heart valves. Circulation 121:1848–1857

47. Zioupos P, Barbenel JC, Fisher J (1994) Anisotropic elasticity and strength of glutaraldehyde fixed bovine pericardium for use in pericardial bioprosthetic valves. J Biomed Mater Res 28:49–57